High-resolution computational modelling of multi-material flows

E. Shapiro*, D. Drikakis

Fluid Mechanics and Computational Science Group, School of Engineering, Cranfield University, Cranfield, MK43 OAL, UK

Abstract

The paper concerns the development of high-resolution methods for variable density flows and the implementation in multi-species flow studies in microfluidics. The high-resolution discretisation is obtained by numerically reconstructing the flow variables using information for the eigenstructure of the system of equations. Three variants of high-resolution methods are presented and their accuracy is assessed against analytic and experimental results for diffusion broadening in microfluidics. Results from numerical convergence studies are also presented to demonstrate the relative efficiency of the three reconstruction variants in conjunction with first-, second and third-order of accuracy in spatial discretisation.

Keywords: High-resolution schemes; Variable density flows; Microfluidics

1. Introduction

The development of advanced computational models for variable density flows is motivated by several application problems spanning from chemical reactors, multi-material mixing and environmental flows, to combustion engineering, biological flow and mass transport. Depending on the application, variable density flows can feature low or high speeds, and a range of spatial and time scales, as well as large density and temperature gradients, which in association with fast chemical reaction rates can result in stiff numerical solutions and slow convergence rates. None of the existing computational methods can be considered as a panacea across the broad spectrum of applications, thus further computational development and investigation are motivated.

During the last few years, high-resolution methods have attracted the interest of computational modellers in a number of applications. A detailed account of the theory, numerical design practices and computational implementation of high-resolution methods for incompressible and low-speed flows can be found in [1]. High-resolution methods essentially constitute advanced computational models, which are designed to satisfy a number of numerical properties that are closely associated with the fluid mechanics and thermodynamics laws. Using this solid computational framework, in the present work we extend a family of high-resolution methods, known as the characteristics-based scheme [1,2], to low-speed, multi-material flows and investigate accuracy and efficiency issues against analytic and experimental data for the problem of diffusion broadening in microfluidic channels.

2. High-resolution method for variable density flows

We consider a variable density multifluid (N species) incompressible flow. The partial densities and total density are denoted by ρ_k, where $k = 1 \ldots N$, and $\rho = \Sigma\rho_k$, respectively. Coupling of the momentum and continuity equations is obtained by the artificial compressibility approach [3], which introduces a pseudo-time pressure derivative, with respect to a pseudo-time τ, to the continuity equation. The system of equations in conservative form and generalised curvilinear co-ordinates (ξ, η, ζ) is then written as

$$\frac{\partial \bar{\mathbf{U}}_p}{\partial \tau} + \frac{\partial \bar{\mathbf{E}}}{\partial \xi} + \frac{\partial \bar{\mathbf{F}}}{\partial \eta} + \frac{\partial \bar{\mathbf{G}}}{\partial \zeta} = -\frac{\partial \bar{\mathbf{U}}_r}{\partial t} + \frac{\partial \bar{\mathbf{R}}}{\partial \xi} + \frac{\partial \bar{\mathbf{S}}}{\partial \eta} + \frac{\partial \bar{\mathbf{L}}}{\partial \zeta} \qquad (1)$$

where $\mathbf{U}_p = (p/\beta, \rho u, \rho v, \rho w, \rho, \rho_k)$ and $\mathbf{U}_r = (0, \rho u, \rho v, \rho w, \rho, \rho_k)$; u, v and w are the velocity components; t and τ are the real and pseudo-time, respectively; and β is the artificial compressibility parameter. The fluxes are given by

* Corresponding author. Tel.: +44 (1234) 754763; Fax: +44 (1234) 758207; E-mail: e.shapiro@cranfield.ac.uk

Computational Fluid and Solid Mechanics 2005
K.J. Bathe (Editor)

$$\begin{cases} \mathbf{E} = (u, \rho u^2 + p, \rho uv, \rho uw, \rho u, \rho_k u) \\ \mathbf{F} = (v, \rho uv, \rho v^2 + p, \rho vw, \rho v, \rho_k v) \\ \mathbf{G} = (w, \rho uw, \rho vw, \rho w^2 + p, \rho w, \rho_k w) \\ \mathbf{R} = \left(0, \tau_{xx}, \tau_{xy}, \tau_{xz}, 0, \frac{1}{Pe}\sum_{l=1}^{l=N} D_{l,k}\rho\frac{\partial \rho_k/\rho}{\partial x}\right) \\ \mathbf{S} = \left(0, \tau_{yx}, \tau_{yy}, \tau_{yz}, 0, \frac{1}{Pe}\sum_{l=1}^{l=N} D_{l,k}\rho\frac{\partial \rho_k/\rho}{\partial y}\right) \\ \mathbf{L} = \left(0, \tau_{zx}, \tau_{zy}, \tau_{zz}, 0, \frac{1}{Pe}\sum_{l=1}^{l=N} D_{l,k}\rho\frac{\partial \rho_k/\rho}{\partial z}\right) \end{cases}$$

where the convective bar-fluxes are defined by $\bar{\varepsilon} = J(\mathbf{E}k_x + \mathbf{F}k_y + \mathbf{G}k_z)$, with $\bar{\varepsilon} = \bar{\mathbf{E}}$ and $\bar{\mathbf{F}}$, $\bar{\mathbf{G}}$ for $k = \xi$, η and ζ, respectively. The viscous fluxes are similarly defined, where τ_{xx}, τ_{xy}, ... are the shear stresses. The terms $Pe = U_o L/D$ and $D_{i,k}$ are the Peclet number and relative diffusion coefficient (dimensionless), respectively, where U_o is a reference velocity and D is a reference diffusion coefficient.

The numerical framework employed in this paper is the characteristics-based scheme [2] (see also [1] for more details) that was originally developed for the solution of the incompressible flow equations. Here, we present the extension of the scheme to variable density flows. For the sake of simplicity, we consider two fluids but the analysis can be easily extended to an arbitrary number of materials. We note that the high-resolution reconstruction concerns the convective fluxes. We present the numerical reconstruction for the convective flux $\bar{\mathbf{E}}$, while we note that the result is similarly applied to the other convective flux components. For steady flows, we retain the pseudo-time derivative on the left-hand side of Eq. (1) and drop the real time derivative from the right-hand side. The one-dimensional counterpart of Eq. (1) is then written

$$\begin{cases} \frac{1}{\beta} - \frac{1}{\sqrt{\xi_x^2+\xi_y^2+\xi_z^2}}p_\tau + u_\xi\tilde{x} + v_\xi\tilde{y} + w_\xi\tilde{z} = 0 \\ \frac{1}{\sqrt{\xi_x^2+\xi_y^2+\xi_z^2}}(\rho u)_\tau + (\rho u^2 + p)_\xi\tilde{x} + (\rho uv)_\xi\tilde{y} + (\rho uw)_\xi\tilde{z} = 0 \\ \frac{1}{\sqrt{\xi_x^2+\xi_y^2+\xi_z^2}}(\rho v)_\tau + (\rho uv)_\xi\tilde{x} + (\rho v^2 + p)_\xi\tilde{y} + (\rho uw)_\xi\tilde{z} = 0 \\ \frac{1}{\sqrt{\xi_x^2+\xi_y^2+\xi_z^2}}(\rho w)_\tau + (\rho uw)_\xi\tilde{x} + (\rho vw)_\xi\tilde{y} + (\rho w^2 + p)_\xi\tilde{z} = 0 \\ \frac{1}{\sqrt{\xi_x^2+\xi_y^2+\xi_z^2}}(\rho)_\tau + (\rho u)_\xi\tilde{x} + (\rho v)_\xi\tilde{y} + (\rho w)_\xi\tilde{z} = 0 \\ \frac{1}{\sqrt{\xi_x^2+\xi_y^2+\xi_z^2}}(\rho_1)_\tau + (\rho_1 u)_\xi\tilde{x} + (\rho_1 v)_\xi\tilde{y} + (\rho_1 w)_\xi\tilde{z} = 0 \end{cases} \quad (2)$$

where $\tilde{k} = \xi_k \Big/ \sqrt{\xi_x^2 + \xi_y^2 + \xi_z^2}$, $k = x, y, z$. This form does not correspond exactly to the physical form of the equations in non-conservative form because the equations for densities contain a velocity divergence part. In non-conservative form the equations for densities will be given by

$$\begin{cases} \frac{1}{\sqrt{\xi_x^2+\xi_y^2+\xi_z^2}}\rho_\tau + \rho_\xi(u\tilde{x} + v\tilde{y} + w\tilde{z}) = 0 \\ \frac{1}{\sqrt{\xi_x^2+\xi_y^2+\xi_z^2}}\rho_{1\tau} + \rho_{1\xi}(u\tilde{x} + v\tilde{y} + w\tilde{z}) = 0 \end{cases} \quad (3)$$

Using Eqs (3), Eqs (2) can be written in three different formulations:

1. **Transport form**, which employs the equations for densities as transport equations (3) and use these to eliminate the total density from the momentum equations of the conservative system (2).
2. **Hybrid form**, which uses the conservative form of the continuity equation in order to eliminate the total density from the momentum equations (2) and then solve the momentum equations coupled with the transport equations for densities (3).
3. **Conservative form**, which, directly, solves the conservative system of Eqs (2).

The three formulations lead to different variants of numerical reconstruction, which are briefly presented below.

2.1. Transport form

Using the same solution procedure as in [1,2], the transport form leads to a system with distinct eigenvalues $\lambda_{0,1,2} = (\lambda_0, \lambda_0 + s, \lambda_0 - s)$, where $s = \sqrt{\lambda_0^2 + \beta/\rho_0}$ is the artificial speed of sound and $\lambda_0 = u_0\tilde{x} + v_0\tilde{y} + w_0\tilde{z}$. Equation (2) leads to the following reconstruction for the primitive variables

$$\begin{cases} p = \frac{1}{2s}(\lambda_1 p_2 - \lambda_2 p_1 - \beta\,(R_1 - R_2)) \\ u = u_0 + \frac{\tilde{x}}{2s\rho_0}R_3 \\ v = v_0 + \frac{\tilde{y}}{2s\rho_0}R_3 \\ w = w_0 + \frac{\tilde{z}}{2s\rho_0}R_3 \\ \rho = \rho_0 \\ \rho_1 = \rho_{10} \end{cases}$$

where the auxiliary functions R_1, R_2 and R_3 are given by

$$\begin{cases} R_1 = \tilde{x}(u_0 - u_1) + \tilde{y}(v_0 - v_1) + \tilde{z}(w_0 - w_1) \\ R_2 = \tilde{x}(u_0 - u_2) + \tilde{y}(v_0 - v_2) + \tilde{z}(w_0 - w_2) \\ R_3 = p_1 - p_2 + \lambda_2\rho_0 R_2 - \lambda_1\rho_0 R_1 \end{cases}$$

The variables $(\rho, p, u, v, w)_{0,1,2}$ are determined from the previous iteration in pseudo-time according to the sign of the corresponding eigenvalue.

2.2. Hybrid form

The hybrid form leads to a system with eigenvalues $\lambda_{0,1,2} = (\lambda_0, (\lambda_0 + s)/2, (\lambda_0 - s)/2)$ and artificial speed of sound $s = \sqrt{\lambda_0^2 + 4\beta/\rho_0}$. The primitive variables are given by

$$\begin{cases} p = \frac{1}{s}(\lambda_1 p_2 - \lambda_2 p_1 - \beta\,(R_1 - R_2)) \\ u = u_0 + \frac{\tilde{x}}{s\rho_0} R_3 \\ v = v_0 + \frac{\tilde{y}}{s\rho_0} R_3 \\ w = w_0 + \frac{\tilde{z}}{s\rho_0} R_3 \\ \rho = \rho_0 \\ \rho_1 = \rho_{10} \end{cases}$$

2.3. Conservative form

The conservative form yields a system with the same eigenvalues as in the hybrid form; however, the reconstructed values for densities include pseudo-compressibility effects,

$$\begin{cases} p = \frac{1}{s}(\lambda_1 p_2 - \lambda_2 p_1 - \beta\,(R_1 - R_2)) \\ u = u_0 + \frac{\tilde{x}}{s\rho_0} R_3 \\ v = v_0 + \frac{\tilde{y}}{s\rho_0} R_3 \\ w = v_0 + \frac{\tilde{z}}{s\rho_0} R_3 \\ \rho = \rho_0 + \frac{\rho_0}{\beta}\left(p - p_0 + \frac{\lambda_0}{s} R_3\right) \\ \rho_1 = \rho_{10} + \frac{\rho_0}{\beta}\left(p - p_0 + \frac{\lambda_0}{s} R_3\right) \end{cases}$$

The eigenvalues for the conservative and hybrid forms correspond to the eigenvalues obtained for a variable-density flow from the direct analysis of the Jacobi matrix (see e.g. [4]).

Finally, the intercell values for $(\rho, p, u, v, w)_{0,1,2}$ are computed by polynomial interpolation up to third-order accuracy [1,2]. For the iteration in pseudo-time we have used a fourth-order Runge-Kutta scheme. Acceleration of the numerical convergence has been obtained by implementing a three-level, full multigrid-full approximation storage algorithm [5].

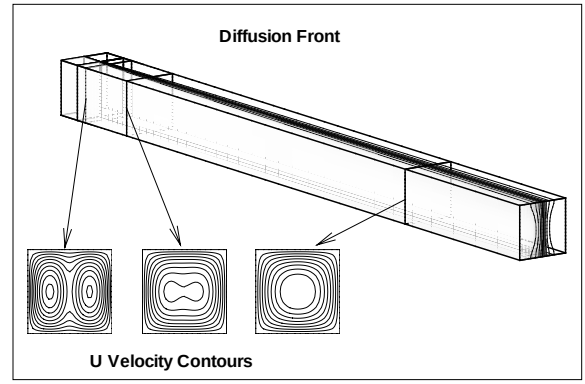

Fig. 1. Development of the flow near the entrance region.

3. Modelling of diffusion broadening in microfluidic channels

In the present paper, we present results from the implementation of the variable density high-resolution method for the problem of diffusion broadening in a microfluidic channel. Two fluids with dimensionless densities 0.8 and 1, respectively, merge through rectangular inlets and flow in a channel with square cross section. The upstream conditions at the inlets are given by parabolic velocity profiles and uniform distribution of densities. The flow domain is illustrated in Fig. 1.

All three numerical reconstruction formulations exhibited the same grid convergence characteristics and there was no significant difference in the accuracy of the obtained results when convergence was achieved: the position of the diffusion front was predicted with a difference less than 0.2%.

On the other hand, the efficiency in terms of multigrid convergence was dependent on the reconstruction

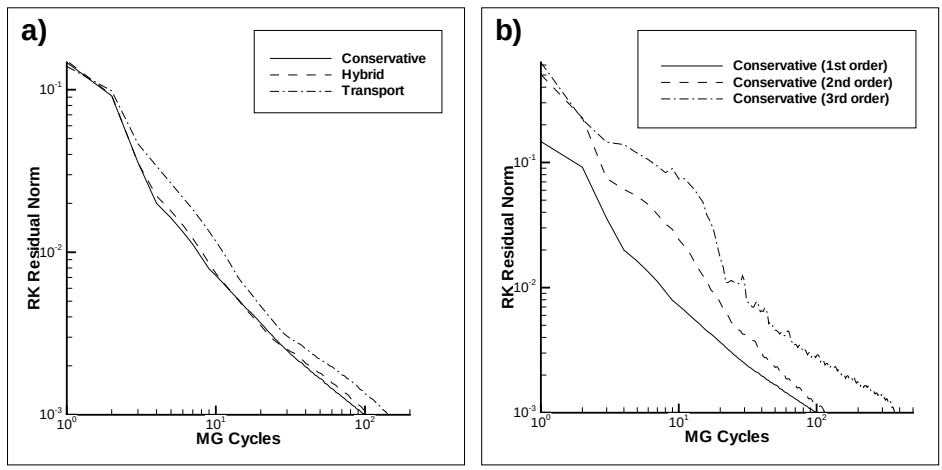

Fig. 2. Multigrid convergence: (a) different high-resolution reconstruction variants; (b) different orders of polynomial interpolation.

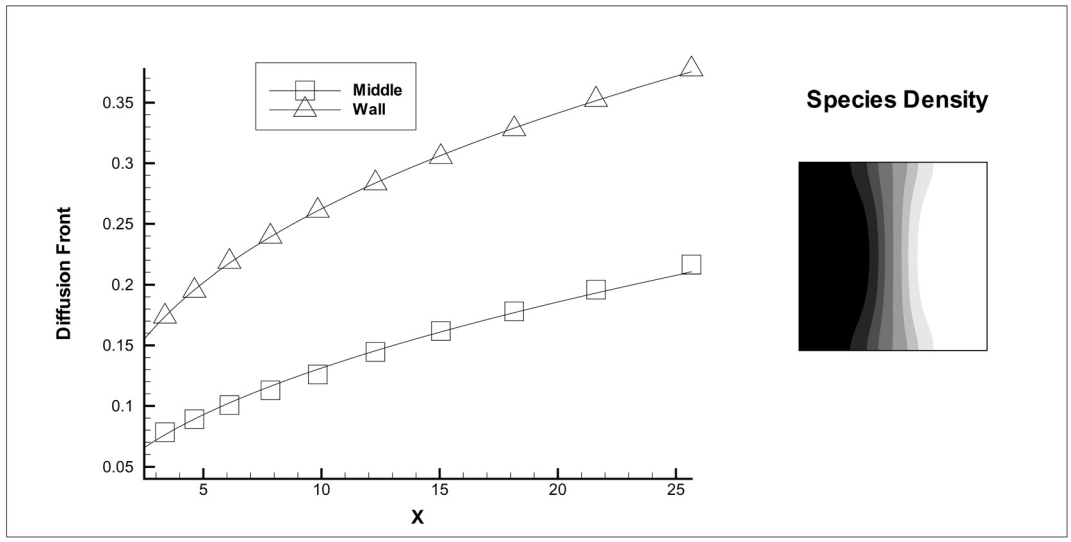

Fig. 3. Development of the diffusion front across the channel. The cross-section plot corresponds to position $x = 20$.

method. Figure 2(a) shows the multigrid convergence for a flow computed at $Re = 25$ using first-order polynomial interpolation and different forms of variables reconstruction. The figure shows the maximum of the solution variation within a pseudo-time step normalised by the maximum variation at the first pseudo-iteration.

The results indicate that the best multigrid convergence is obtained using the conservative form of the variables reconstruction. For example, reduction of the residual by 3 orders of magnitude requires 76, 90 and 124 multigrid cycles for the conservative, hybrid and transport formulations, respectively. Higher-order polynomial interpolation for $(\rho, p, u, v, w)_{0,1,2}$ yielded more accurate results for the flow but required more multigrid cycles to achieve the same level of convergence (Fig. 2(b)). Tests performed at different Reynolds numbers revealed that the numerical convergence is improved at higher Reynolds numbers for all forms of variables reconstruction.

Figure 3 illustrates the development of the diffusion front defined as the point where species density falls below 20% of its density at the inlet. The results obtained by the high-resolution, variable density method for the diffusion broadening slopes were found to be in satisfactory agreement (Table 1) with analytic [6] and experimental results [6,7].

Table 1
Comparison of diffusion broadening slopes between the high-resolution model, analytic and experimental data

	Wall	Middle of the channel
Analytic [6]	0.33	0.5
Experimental [6,7]	0.34	0.49
Numerics	0.38	0.51

4. Concluding remarks

We have presented a high-resolution method for modelling and simulation of variable density, multi-material flows, and have applied it to the problem of diffusion broadening in a microfluidic channel. The three variants of the method provide similar results in terms of accuracy but differ with respect to the convergence. The best convergence results were achieved for the full conservative form. All high-resolution variants exhibit good accuracy against experimental and analytic results.

Acknowledgements

The financial support of the Engineering and Physical Sciences Research Council (GR/S13668) is greatly appreciated.

References

[1] Drikakis D, Rider W. High-Resolution Methods for Incompressible and Low-Speed Flows. Berlin: Springer, 2004.
[2] Drikakis D, Govatsos PA, Papatonis DE. A

characteristic-based method for incompressible flows. Int J Num Methods Fluids 1994; 19(8):667–685.
[3] Chorin AJ. A numerical method for solving incompressible viscous flow problems. J Comput Phys 1967;2:12–36.
[4] Riedel U. Finite-volume scheme on unstructured grids for stiff chemically reacting flows. Combust Sci Tech 1998;135:99–116.
[5] Drikakis D, Iliev OP, Vassileva DP. A nonlinear multigrid method for the three-dimensional incompressible Navier-Stokes equations. J Comput Phys 1998;146:301–321.
[6] Ismagilov RF, Stock AD, Kenis PJA, Whitesides G. Experimental and theoretical scaling laws for transverse diffusive broadening in two-phase laminar flows in microchannels. Appl Phys Lett 2000;76(17):2376–2378.
[7] Greiner KB, Deshpande M, Gilbert JR, Ismagilov RF, Stroock AD, Whitesides GM. Design analysis and 3D measurement of diffusive broadening in a Y-mixer. In: Technical Proceedings of Micro Total Analysis Systems, Enschede, The Netherlands, MicroTAS 2000, pp. 87–90.